AIAA JOURNAL
Vol. 39, No. 4, April 2001

Structural Design of a Silicon Micro-Turbo-Generator

Kuo-Shen Chen*
National Cheng-Kung University, Tainan 70001, Taiwan, Republic of China
S. Mark Spearing†
Massachusetts Institute of Technology, Cambridge, Massachusetts 02139-4307
and
Noel N. Nemeth‡
NASA John H. Glenn Research Center at Lewis Field, Cleveland, Ohio 44135

The probabilistic structural analysis and design of a silicon micro-turbo-generator rotor are presented. This rotor was designed to have a tip speed of 500 m/s. Three-dimensional finite element analysis, fracture strength characterization of single crystal silicon, and structural failure probability calculations were performed. The results show that the design of micro-turbine-generator rotor, although highly stressed, is feasible. However, it is important to note that this feasibility is very dependent on the etching process achieving a high surface quality. The overall approach and tests employed are equally applicable to other highly stressed microelectromechanical systems.

Nomenclature

A = surface area
A_0 = reference area
a = crack length
b = outer radius of disk
C_{ij} = stifness tensor for linear elastic material
E = Young's modulus
K_{I} = stress intensity factor (mode 1)
K_{Ic} = fracture toughness in mode 1 (opening)
M = number of subvolumes per element
m = Weibull modulus
N = number of elements in finite element model
n = number of blades on disk
P_f = probability of failure
P_{fb} = probability of failure of blade
P_{fbr} = probability of failure at blade root
P_{fji} = probability of failure of subvolume ji
r = radial coordinate
S = stress ratio for equal failure probability
u = displacement
V = volume
V_0 = reference volume (Weibull)
Y = geometrical correction for stress intensity factor
θ = circumferential coordinate (angular)
λ = threshold stress (Weibull)
ν = Poisson's ratio
ρ = density
σ_0 = reference stress (Weibull)
$\sigma_{1,2,3}$ = principal stress components
ω = rotational frequency

I. Introduction

A RESEARCH and development program is underway to develop the technology for micro-gas-turbine generator "microengines."[1–4] These are intended to be capable of producing 50 W of electrical power in a package less than 1 cm^3 in volume while consuming 7–8 g of jet fuel per hour. Such devices would represent a quantum leap in compact electric power sources, with the potential to achieve more than 10 times the power and energy density of current batteries at competitive costs.

The concept on which this ultimate goal is based is the ability to micromachine refractory, structural ceramics such as silicon nitride and silicon carbide. These materials potentially have excellent mechanical, thermal, and chemical properties for gas-turbine applications; in principle they would permit uncooled operation in the range of 1500–1700 K.

To appreciate the impact of material scaling on structural design, it is important to have a basic understanding of the functional requirements of a microengine. The most challenging component of the device from a structural viewpoint is the turbine rotor. A cross-sectional view of the turbine is shown in Fig. 1, and a micrograph showing a stator/rotor pair etched from silicon is shown in Fig. 2. The design is quite different from conventional turbomachinery, as it is largely determined by the capabilities of the microfabrication processes. The use of etching and deposition processes in conjunction with lithographically produced masks limits the components to planar or cylindrical geometries. However, this can have the advantage that relatively complicated components can be created out of a single wafer of monolithic silicon, eliminating many of the assembly operations (e.g., attachment of blades) that would be required at the macroscale and that can be a source of reliability concerns. The overall device, and any three dimensionality that is required, is created by bonding together several etched wafers. For the turbine shown in Fig. 1, nine discrete layers would be required, with only eight bonds. As an additional concern, it is difficult to create high-aspect-ratio components such as shafts, and as a consequence the rotor is supported by a novel design of gas bearings.[5]

The demands of high-power-density turbomachinery operation drive the turbine design toward operating at the maximum possible temperature and the maximum possible tip speed of the blades. The stress levels scale with the square of the speed and linearly with the density of the material.[6] Thus the strength at temperature of the material defines the performance of gas-turbine engines at the micro as for the macroscale.

The initial focus of the microengine program is to design and fabricate a turbogenerator from silicon, for which fabrication processes have already been proven. In parallel, development is underway of processes suitable for more refractory materials. Similar structural issues must be addressed for both the silicon turbogenerator and the microengine itself. The fundamental task is to develop and validate a methodology for achieving structurally reliable, highly stressed devices, which are microfabricated from intrinsically brittle materials. This paper describes the structural design and associated material testing for the silicon turbogenerator rotor. The focus is on its

---

Presented as Paper 99-1332 at the AIAA/ASME/ASCE/AHS/ASC 40th Structures, Structural Dynamics, and Materials Conference, St. Louis, MO, 12–15 April 1999; received 28 December 1999; revision received 1 September 2000; accepted for publication 1 September 2000.

*Assistant Professor, Department of Mechanical Engineering, Room 91710.

†Esther and Harold E. Edgerton Associate Professor, Department of Aeronautics and Astronautics.

‡Research Scientist.

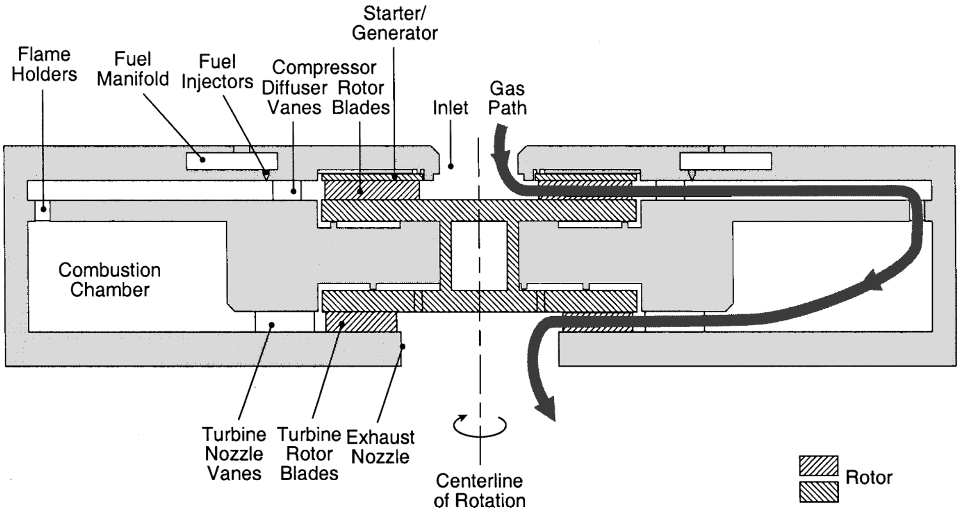

Fig. 1 Baseline design of the microengine in cross section.

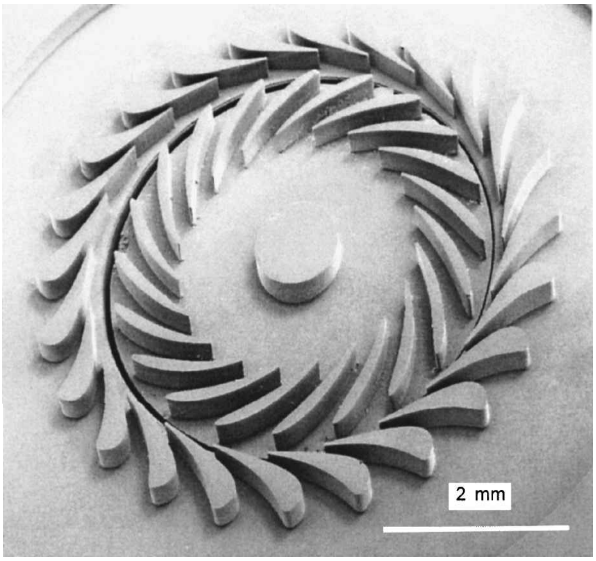

Fig. 2 SEM micrograph of the microturbine, the bladed rotor, and nozzle guide vanes on the stator are clearly visible (courtesy of Chuang-Chia Lin).

room-temperature operation; a separate analysis has been conducted for its high-temperature performance.

II. Background

A. Material Properties

The elastic properties of $\langle 100\rangle$ silicon have been documented.[7] The three components of the elastic stiffness tensor necessary to characterize cubic silicon are $C_{11} = 165.7$ GPa, $C_{12} = 63.9$ GPa, and $C_{44} = 79.6$ GPa. In terms of the engineering elastic constants, the Young's modulus E varies from 169 GPa in the $\langle 110\rangle$ direction to 131 GPa in the $\langle 100\rangle$ direction. The Poisson's ratio ν also varies with orientation; however, the combined quantity $(1-\nu)/E$ is an invariant.

At temperatures below about 600°C, silicon is a brittle, elastic material, which can exhibit an extremely high inert strength.[8] The fracture toughness K_{IC} varies with orientation, but the variation is small and in all cases K_{IC} is less than 1 MPa$\sqrt{\mathrm{m}}$.[9] The low toughness implies a strong sensitivity of the strength to processing and service induced flaws or cracks; nonetheless, several studies have shown that it is possible to obtain strengths in excess of 1 GPa.[10,11] The lack of plasticity implies that cyclic fatigue crack growth is not a concern; however, environmentally assisted slow crack growth can occur.[12]

The deformation behavior of single crystal silicon has been obtained as a function of temperature by Mura et al.[13]; their results show that the stress/strain relationship is essentially unaffected by temperatures below 600°C. Above 800°C distinct yield phenomena were observed. The brittle-to-ductile transition temperature (BDTT) of silicon 550°C is well defined, with a weak dependence on stress state.[14] Above the BDTT plastic deformation becomes more prevalent until at temperatures above 800°C it is the strength-limiting process. The BDTT clearly defines the applicable temperature regimes for both brittle or ductile structural design methodologies for devices using single crystal silicon.

B. Fabrication Constraints

The fabrication of the silicon turbogenerator is enabled by deep reaction ion etching (DRIE) using a Surface Technology Systems™ (STS) inductively coupled plasma etcher.[15] The equipment is characterized by a high-density plasma and achieves an etch rate of ~3 μm/min in silicon. In contrast to macroscale machining processes which can more readily produce three-dimensional geometries, the microfabrication process is limited to two-dimensional extruded shapes. As a result, traditional methods for minimizing stress levels, such as radially varying the disk thickness and tapering blades, cannot be used. This is a major structural design constraint for microturbomachinery. In addition, the high aspect ratios of the blades and journal bearing gap demand a fast and highly anisotropic etching process. This introduces difficulties in creating fillets for stress relief at sharp transitions between horizontal and vertical features. Furthermore, scanning electron microscopy (SEM) indicates that the surface quality is worse in these transition regions. This poorer surface can result in a locally inferior material strength.

C. Fracture Mechanics and Weibull Statistics

In 1920 Griffith proposed a fracture theory to describe the behavior of materials with microcracks.[16] The Griffith energy balance criterion for fracture states that crack growth will occur if the energy release rate reaches a critical value. This criterion can be recast in terms of a stress-based parameter; the stress intensity factor K_I, which is defined as

$$K_I = \sigma_\infty Y \sqrt{\pi a} \tag{1}$$

where Y is the shape factor which is usually close to unity. If K_I is larger than K_{IC}, the fracture toughness of the material, the crack will propagate and the structure fails. The key consequence of Eq. (1) is that K_I is determined by both the state of stress and the flaw size. In brittle materials the critical flaw sizes are usually below the capabilities of nondestructive evaluation techniques and are generally accounted for using a probabilistic stress-based design methodology.

The most widely used approach to account for the stochastic nature of the strength of brittle structures is the weakest link model.[17] In this model the failure probability of a volume of material V under a uniform stress σ is assumed to be given by

$$P_f(\sigma, V) = 1 - \exp\{-(V/V_0)\ (\sigma - \lambda)/\sigma_0]^m\} \tag{2}$$

where λ is a threshold parameter, which corresponds to the minimum material strength. For ceramics λ is often taken to be zero. This leads to the two-parameter Weibull distribution

$$P_f(\sigma, V) = 1 - \exp[-(V/V_0)(\sigma/\sigma_0)^m] \tag{3}$$

Depending on the nature of the strength controlling flaw population, the failure probability can also be treated as surface area dependent. In which case an area term A/A_0 is substituted for V/V_0. The failure type (volume or surface flaw) can be determined by a combination of fractography, finite element analysis, process characterization, and material properties. Similarly, the choice between a two- and three-parameter Weibull model depends on the nature of the strength distribution and the statistical level of confidence required.

Equations (2) and (3) are suitable for uniform uniaxial tensile stress. For uniform multiaxial stress states the Weibull distribution must be modified. The principle of independent action model[18] states that the Weibull survival probability of a uniformly stressed material element experiencing multiaxial loading is equal to the product of the survival probabilities for each of the tensile principal stresses applied individually, i.e., Eq. (3) can be rewritten as

$$P_f(\sigma, V) = 1 - \exp\{-(V/V_0)[(\sigma_1/\sigma_0)^m + (\sigma_2/\sigma_0)^m + (\sigma_3/\sigma_0)^m]\} \tag{4}$$

In general, the principal stresses vary with position, thus Eq. (4) must be integrated over the volume or surface area of the structure in order to obtain the overall failure probability. The finite element method is a convenient means of achieving this integration.

Consider a finite element model of a structure. The structure is discretized into N finite elements. Each finite element has M Gaussian integration points with M associated subvolumes, each with a unique set of principal stresses.

The probability of failure of each Gaussian subvolume P_{fji} can be directly calculated via Eq. (4). The overall structural failure probability is obtained by the following product:

$$P_f = 1 - \sum_{i=1}^{N} \sum_{j=1}^{M} (1 - P_{fji}) \tag{5}$$

Probabilistic structural design has been used for the silicon microturbine. As shown in Fig. 3, the procedure consists of two pretasks conducted in parallel: material characterization to extract the statistical material parameters and finite element analysis to perform the structural stress-volume integration. Based on this information, the structural failure probability is then calculated. If the overall failure probability exceeds an allowable value, the structural design must be modified.

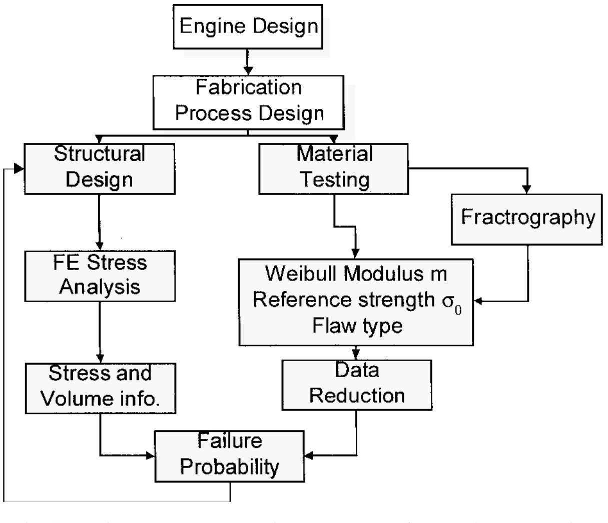

Fig. 3 Brittle structural design procedure for a brittle material.

III. Stress Analysis

A. Preliminary Design

The baseline rotor geometry was obtained by trading between turbomachinery performance and the capabilities of the fabrication process.[3] The rotor is a 4-mm-diam, 300-μm-thick disk with blades on one side. The design tip speed is 500 m/s, corresponding to a rotational speed of 2.5×10^6 rpm. The stress and deformation of a flat rotating disk made from a homogeneous isotropic linear elastic material with radius b can be found[6] as a function of radial coordinate r, rotational speed ω, density ρ, Young's modulus E, and Poisson's ratio ν:

$$\sigma_r = (3 + \nu)/8]\rho\omega^2(b^2 - r^2) \tag{6}$$

$$\sigma_\theta = (3 + \nu)/8]\rho\omega^2 b^2 - (1 + 3\nu)/8]\rho\omega^2 r^2 \tag{7}$$

$$u = (1 - \nu)/8E]\ (3 + \nu)\rho\omega^2 b^2 r - (1 + \nu)\rho\omega^2 r^3] \tag{8}$$

where σ_r, σ_θ, and u are the radial stress, hoop stress, and radial expansion, respectively. For more complicated geometries or nonisotropic material properties solutions can be obtained by numerical analysis such as the finite element method.

By Eqs. (6) or (7) the maximum stress in a flat 4-mm-diam silicon disk rotating at 2.5×10^6 rpm is 240 MPa. The radial growth, calculated by Eq. (8), is 1.5 μm. These stress and deformation levels are well within the design allowables for silicon and satisfy the requirement of maintaining a journal bearing gap within tight tolerances. The preliminary calculation, therefore, provided confidence to proceed with more detailed analysis.

B. Axisymmetric Finite Element Analysis

As shown in Fig. 2, the baseline turbine disk design has 20 blades. A raised central hub is used to carry the thrust bearing loads. To establish a basis for design trades without incurring the cost of a full three-dimensional finite element (FE) analysis, a two-dimensional axisymmetric model was used as an intermediate step. The commercial finite element package, ABAQUS™ Standard, was used for this purpose.[19]

There are potentially three stress critical locations on the rotor: the disk center, the junction between the hub and the disk, and the junctions between the disk and the turbine blades. The asymmetric location of the blades on one side of the disk implies that not only the radial expansion, but also the out-of-plane deflection, must be considered. To account for this, the blades were represented by an axisymmetric "lumped" mass.

Figure 4 shows the lumped geometry of the baseline turbine disk. The lumped mass is obtained by matching the total mass and rotational inertia of the turbine blades in order to generate the same radial stresses at the hub and tip deflections. The height of the annular mass was maintained as the same as the blade height, with the radial dimension and location being varied in order to match the mass and inertial properties of the blades. This model was verified subsequently by comparison to a full three-dimensional model described in Sec. III.C.

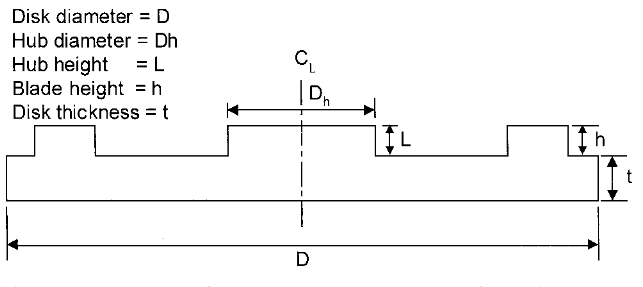

Fig. 4 Axisymmetric finite element representation of the micro-turbo-generator rotor.

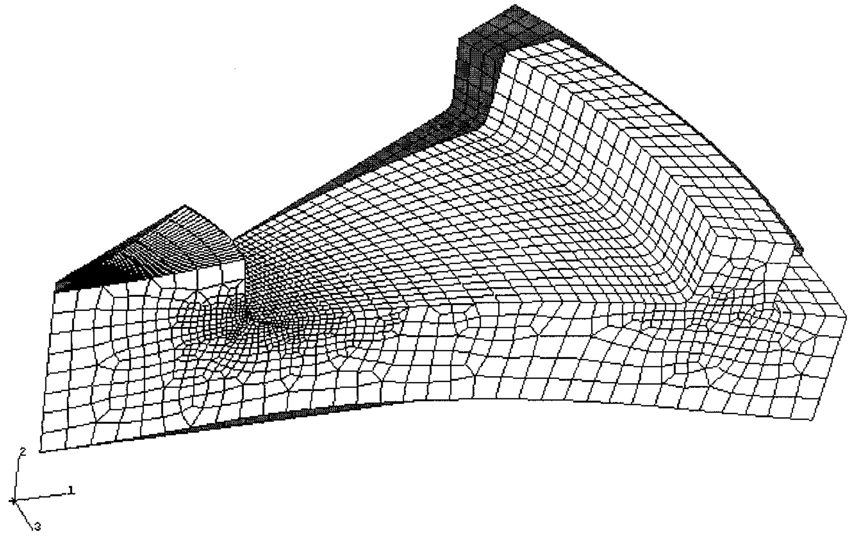

Fig. 5 Deformation of the axisymmetric model subjected to centrifugal force.

Figure 5 shows the deflections at the outer radius of the rotor as a function of blade height and disk thickness. For the baseline 200-μm tall blades, a 2.4-μm vertical deflection at the disk tip was calculated. The radial expansion is 1.5 μm, which is essentially the same as that calculated for an unbladed disk. The stress level at the disk center is also close to the flat disk case. However, the stress distribution is quite different. The top surface of the disk, subject to a centrifugal and a tensile bending stress, shows a higher stress level than the bottom surface, which is subjected to a centrifugal and a compressive bending stress.

Two parametric studies were performed using the axisymmetric model. These explored, first, the relationship between disk thickness, blade height, and tip deflection, and second, the relationship between fillet radius, hub aspect ratio, and the stress concentration at the hub/disk fillet. Figures 6a and 6b show the relationships between disk thickness, blade height, and out-of-plane deflection. This is an important design trade because the out-of-plane deflection must be minimized in order to achieve the required thrust bearing performance. Figure 6 shows that this can be achieved by reducing the blade height and increasing disk thickness. This conflicts with the demands of turbomachinery performance, which drive the design toward taller blades, and it also partly conflicts with the fabrication considerations, which restrict the design to thinner disks and shorter blades in order to minimize etching cycle times.

The sensitivity of the stress concentration at the hub/disk interface to the design variables is shown in Fig. 7. Figure 7a shows the effect of placing the blades asymmetrically on one side of the disk as opposed to having a balancing mass on the reverse side of the disk. The stress level in the asymmetric case is larger as a result of the contribution of the bending moment. Figure 7b shows that the stress concentration at the hub/disk transition is a strong function of the local fillet radius. The stress is reduced by 40% if the fillet radius is increased from 10 to 30 μm. A higher fillet radius is clearly desirable; however, this significantly increases the fabrication complexity. The analysis also shows that the stress concentration is a weak function of the hub height L.

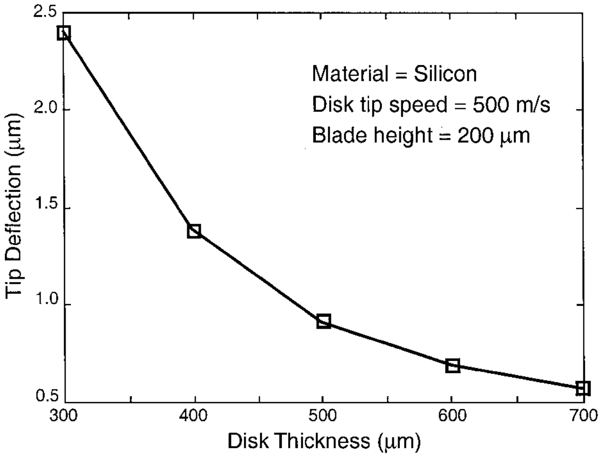

Fig. 6a Relationship between rotor deflection and rotor thickness.

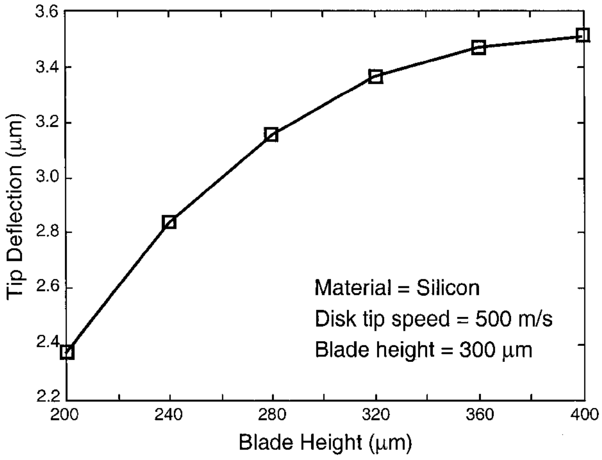

Fig. 6b Rotor deflection vs blade height.

C. Three-Dimensional Finite Element Analysis

The two-dimensional analysis provides useful input to the design process; however, the turbine geometry is not axisymmetric, and furthermore, silicon has cubic material symmetry. Consequently, a three-dimensional FE analysis was used for detailed design. In particular, the following issues were addressed: 1) the effect of material anisotropy, 2) the state of stress around the turbine blades, and 3) the structural dynamics of blade and disk.

Figure 8 shows a three-dimensional FE mesh of the whole microrotor. This corresponds to the rotor shown in Fig. 2, with the stator parts omitted. Figure 9 shows the relationship between deformation and rotating speed in both axisymmetric and full three-dimensional models. The axisymmetric model underpredicts the deformation by about 25%. This discrepancy is not surprising because the axisymmetric model was initially designed only to provide estimates before embarking on a more detailed analysis. The blades were lumped to maintain the same rotational inertia, which would contribute the same stress level to the disk center and hub/disk interface but not necessarily the same stiffness and hence tip deflection.

To determine the blade-root stress, a more detailed model was constructed. The critical point is at the root of the trailing edge of the blades. Figure 10 shows the corresponding FE mesh and calculated stress contours.

A parametric study was conducted to examine the relationship between blade stress, blade height, and blade-root fillet radius. Figure 11 presents the results of this parametric study. The maximum stress at the critical point triples as the blade height is doubled. This is because of the centrifugal bending of the blade. The fillet radius must be increased in order to reduce the stress level if the blade height is to be increased. As for the axisymmetric analysis, these results help guide the design tradeoff between turbomachinery performance, fabrication process, and structural integrity. Mesh refinement studies were conducted on the models shown in Figs. 8 and 10. The displacements in Fig. 9 were estimated to be accurate to within 2%, and the stresses shown in Fig. 11 were estimated to be accurate to within 3%.

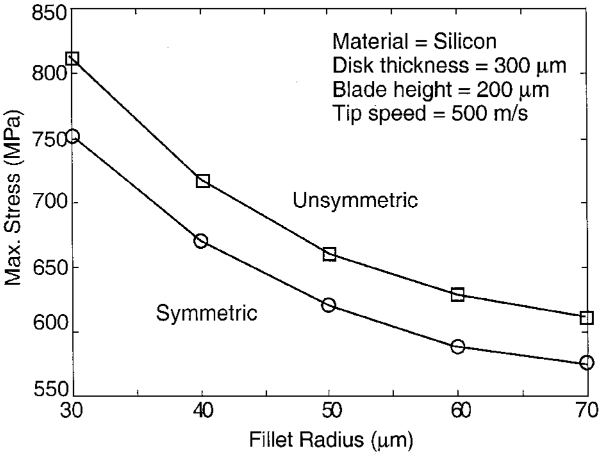

Fig. 7a Effect of out-of-plane asymmetry on the hub root stress concentration.

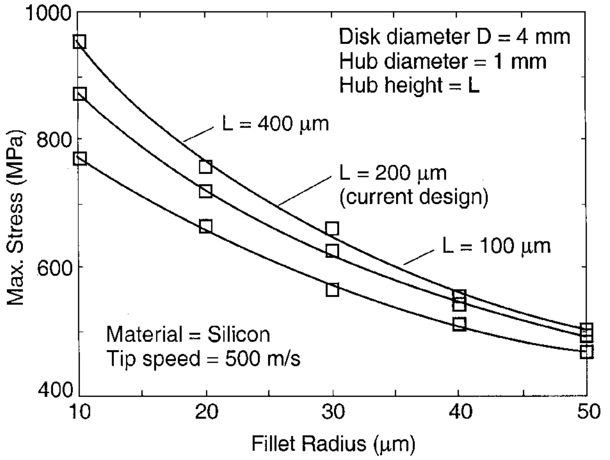

Fig. 7b Relationship between stress concentration, fillet radius, and aspect ratio (*L*/*D*).

The effect of anisotropy was examined by applying the cubic material properties to a FE model of a flat rotating disk, using the orthotropic material option available within ABAQUS™. The calculation shows that the anisotropic model has a 3% increasing in maximum stress over the isotropic case. The ⟨110⟩ direction has the highest stress for a given radius. The radial expansion, however, is independent of direction, which follows from Eq. (3), which shows that the expansion depends on the invariant property $1 - \nu/E$. This analysis indicates that use of isotropic material properties is a good approximation even for detailed analysis.

The resonant frequencies essentially scale inversely with length.[20,21] Moreover, in comparison with large-scale turbomachinery, the microturbine blades have relatively low aspect ratios. These two factors imply that the microturbine blades will have extremely high resonant frequencies. Although the rotating speed also increases, the extremely high resonant frequencies and small number of blades results in an unusually high operating margin between the turbomachinery frequency and the first structural mode. At 500 m/s tip speed the turbomachinery excitation frequency is nearly 0.9 MHz, whereas the first structural natural frequency is 2.5 MHz. This advantage occurs even though centrifugal stiffening is relatively unimportant in microturbomachinery.[22] Figure 12

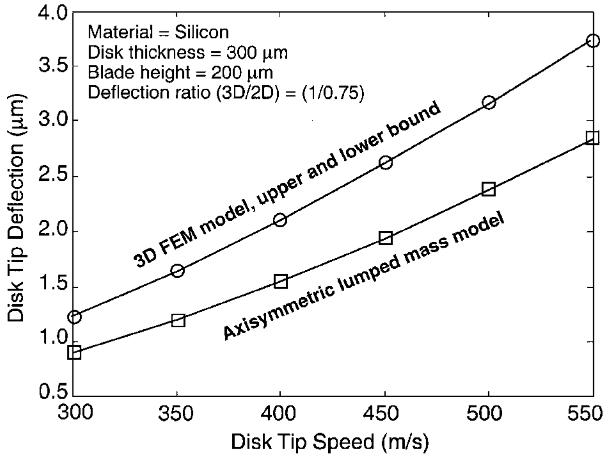

Fig. 9 Relationship between deflection and rotating speed.

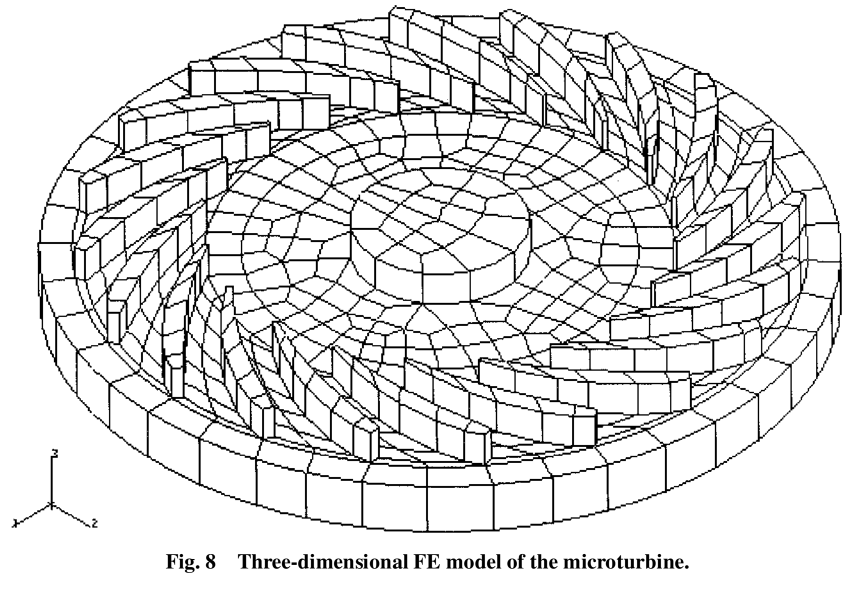

Fig. 8 Three-dimensional FE model of the microturbine.

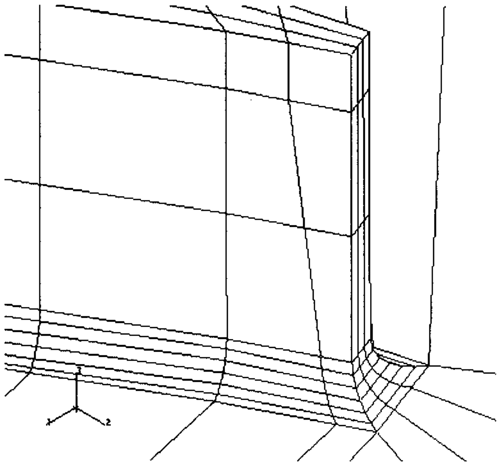

FE mesh

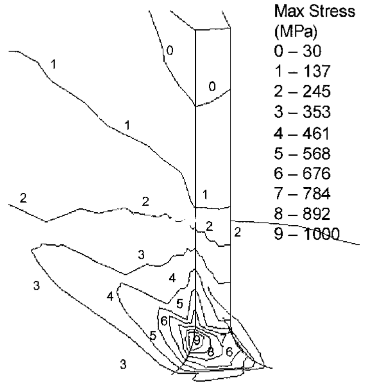

Stress contour

Fig. 10 FE model to calculate the blade-root-stress concentration.

shows the first, the second, and the third modes of the turbine blades. Dynamic effects do limit the rotor design in other respects as the stiffness of the micro-gas bearing is much less than that of the turbine disk. As a result, the first several modes of the turbine disk are essentially rigid-body motions with frequencies much lower than the operating speed of the engine. The issues arising from this are describe elsewhere.[23] The low aspect ratio of the blades implies that the steady-fluid loading results in a negligible contribution to the overall stress level compared to the centrifugal loading.

IV. Material Characterization

The analysis presented in Sec. III shows that the local stress levels in the microturbine are of the order of 1 GPa. This places severe demands on the strength of the silicon and hence on the fabrication route, which controls the surface flaw distribution. To establish the material strength distribution, it is necessary to conduct tests on specimens fabricated by the same etching process as the rotor itself. Furthermore the test specimens should have a similar volume or surface area under stress as in the microengine in order to avoid excessive extrapolation of the calculated Weibull parameters. This section summarizes the results of a comprehensive mechanical test program. The results are described in detail elsewhere.[24,25]

To find the relationship between material strength and surface processing route, biaxial flexure specimens were tested. Figure 13 shows schematically the testing apparatus. Applied load was monitored by a load cell and recorded digitally via a data acquisition system. A FE analysis was conducted to establish the stress/load conversion for the specimen. The strength is determined by the stress at the maximum load. Table 1 summarized the biaxial testing results. The reference strength ranges from 1.6 GPa for mechanically ground specimens to 4.6 GPa for STS DRIE specimens. The Weibull modulus ranges from 3 to 12, which is lower than that commonly achieved by conventional polycrystalline ceramic processing routes.

Table 1 Summary of the biaxial flexure specimen strengths

Variable	Ground (a)	Ground (b)	KOH etched	STS DRIE	Polished
Size	19	30	25	20	10
Thickness	500 μm	280 μm	280 μm	230 μm	280 μm
Surface roughnes	~3 μm	~1 μm	~0.3 μm	~0.3 μm	~0.1 μm
σ_0	1.2 GPa	2.2 GPa	3.5 GPa	4.6 GPa	>4 GPa
m	2.7	3.4–4.2	7.2–12	3.3	——

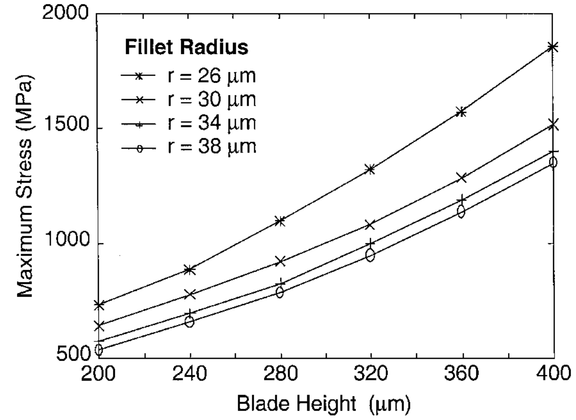

Stress vs blade height

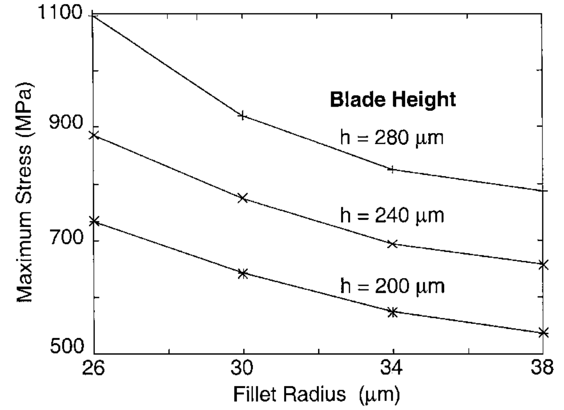

Stress vs fillet radius

Fig. 11 Relationship between blade-root-stress concentration and design parameters.

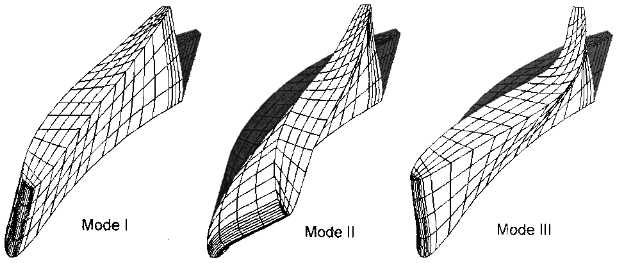

Fig. 12 First three vibration modes of a turbine blade.

Observations of DRIE silicon parts show that the surface quality varies significantly with the conditions used to etch the specimens and also with the location within each specimen. Figure 14 is a SEM micrograph of the hub/disk interface. At the disk/blade and disk/hub transition the surface is rougher than the planar surface of the rotor. This increased roughness results in a reduced strength. Unfortunately, the hub and blade roots are stress concentrations;

Table 2 Summary of the DRIE RHFS strengths

Variable	STS RHFS	STS RHFS + wet etch	STS RHFS + SF_6 dry etch
Sample size	35	31	28
Post DRIE etch depth	NA	1.8 μm	2.7 μm
σ_0	1.5 GPa	2.9 GPa	4 GPa
m	9.04	4.3-5.3	3.3-8.8

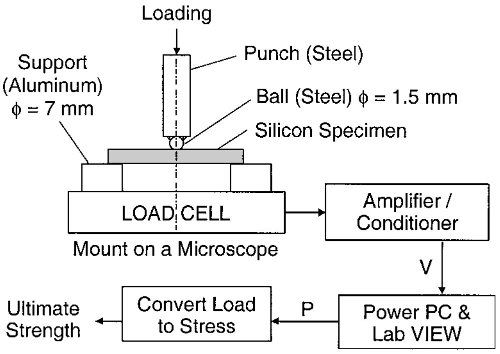

Fig. 13 Strength testing procedure.

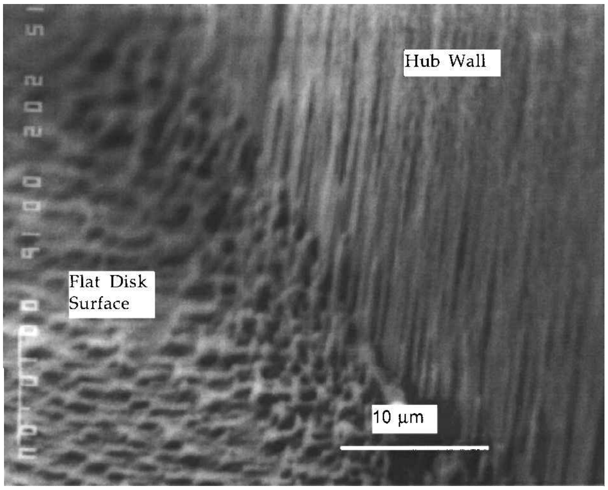

Fig. 14 SEM image of the turbine surface.

therefore, the reduced local surface quality, and associated reduction in strength, has potentially serious consequences for the design and operation of the rotor. To achieve a successful design, it is necessary to understand the factors affecting the local strength and also to develop techniques to improve the strength by controlling the etched surfaces at critical locations. To characterize the local variation in strength and to explore methods for strength control, a novel specimen has been developed: the radiused hub flexure specimen (RHFS). Readers are referred to Ref. 24 for a more detailed description of the specimen geometry. Test results obtained using the RHFS are presented in Table 2. The local roughness results in a reduction in strength by approximately a factor of three. However, these results also illustrate that the use of a secondary etch to reduce the surface roughness can result in a significant recovery of the strength. The utilization of such techniques to ensure high strength are an important consideration in the design and manufacture of high-power density microelectromechanical systems (MEMS).

V. Failure Probabilistic Analysis

Based on the information of Secs. III and IV, the structure failure probability can be calculated. For this purpose a reference strength of 3.5 GPa and a Weibull modulus of 10 were used. These correspond to the test results for KOH-etched biaxial specimens and hence represent a realistic estimate for what can be achieved with a DRIE followed by a strength recovering secondary etch.

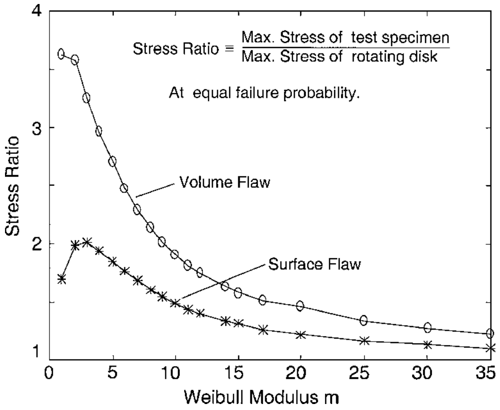

Fig. 15 Stress ratio between the mechanical test specimen and rotating disk as a function of Weibull modulus.

A. Tested /Design Strength Conversion

Because the volume and surface area of the tested specimen are different than that of the microturbogenerator, the reference strength obtained in Sec. V must be scaled before it can be applied to structural design. To illustrate the scaling of strength, it is convenient to introduce a stress ratio S which is arbitrarily defined as the ratio of the maximum stress in the mechanical test specimen to the maximum stress in the structure, which gives the same probability of failure for the two cases:

$$S \equiv \frac{(\sigma_{\max})_{\text{specimen}}}{(\sigma_{\max})_{\text{structure}}} \tag{9}$$

This stress ratio S is a function of the form of the stress distributions and the dimensionless variables A/A_0, σ_l/σ_0, and m. Figure 15 plots the stress ratio between the test specimen and a rotating disk with the same diameter as the microturbine rotor. For comparison, results are shown for both volumetric and surface flaw distributions. Refer to Ref. 24 for a detailed derivation. The key implication of Fig. 15 is that for these particular test specimens and structural geometries the allowable stresses in the structure are significantly lower than those measured in the mechanical tests. For instance, for specimens with a measured Weibull modulus of 10 the stress ratio is 1.5. This implies that the stress level must be scaled by a factor of 0.67 (1/1.5) to achieve an equal probability of survival in the rotating structure. For more complicated geometries, where analytical solutions are not possible, the stress ratio can be obtained by numerical methods. For the detailed structural design the CARES/LIFE code developed by NASA[23,26] was used in conjunction with ABAQUS for finite element analysis.

B. Parametric Studies

Because the centrifugal stress varies with the square of the tip speed, as the rotating speed increases, the failure probability also increases. Figure 16 shows the calculated dependence of failure probability on rotating speed. The geometries investigated in this study were initially restricted to a flat disk and a flat disk with a central hub, in each case with the same dimensions as the baseline design. Both volumetric and surface flaw-dominated cases were calculated for comparison, although it is believed that the structural behavior is dominated by surface flaws. As shown in Fig. 16, for a rotating disk the failure probability of a surface flaw-dominated situation is less than the corresponding probability in a volumetric flaw-dominated situation. However, for the case of a disk with a central hub with a 15-μm fillet radius the failure probability increases. Conversely, the corresponding volumetric flaw-dominated failure probability does not change significantly. The 15-μm fillet radius at the hub-disk transition represents a significant stress concentration. The ratio of this area of locally high stress to the overall surface area is much larger than the ratio between the stress concentrated volume

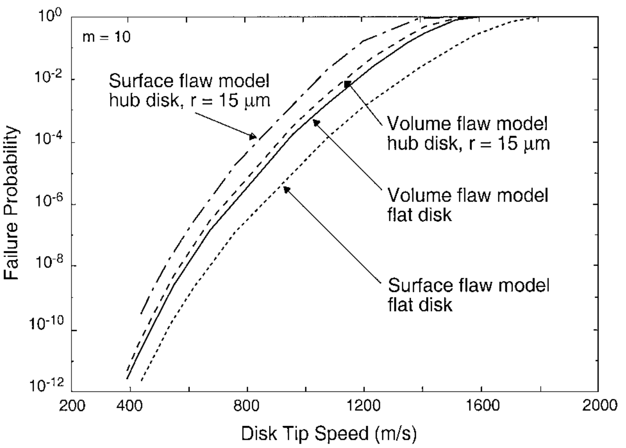

Fig. 16 **Relationship between structure failure probability and rotating speed.**

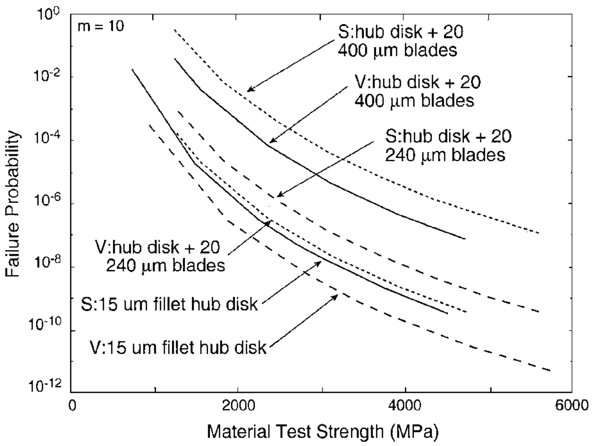

Fig. 17 Relationship between structure failure probability and blade height. (Note: in this figure V stands for volume flaw model, and S stands for surface flaw model.)

to the overall material volume. As a result, this stress concentration is significant in the surface flaw-dominated case but less important in the volumetric flaw-dominated case.

It is more difficult to perform directly a parametric study of the full bladed disk because the mesh size would be too large if the necessary refinement were implemented at the root of each blade. However, a good approximation can be obtained by combining the calculation for the failure probability of a single blade with that for the failure probability of a disk with a central hub. Because the effect of anisotropy is small and each blade is geometrically identical, the failure probability for each blade is essentially the same. In addition, from the stress analysis, except at the blade root, the body of a blade has very low stress level. Letting the failure probability of a single blade and its root be P_{fb} and P_{fbr}, respectively, then

$$P_{\mathrm{fbr}} \approx P_{\mathrm{fb}} \tag{10}$$

By weakest link statistics the total failure probability P_{ftotal} of the blade set is, therefore,

$$P_{\mathrm{ftotal}} = 1 - (1 - P_{\mathrm{fbr}})^N \tag{11}$$

where N is the number of blades.

As P_{fbr} is small ($<10^{-2}$), Eq. (11) can be approximated by the linear term of the bilinear expansion, i.e.,

$$P_{\mathrm{fbtotal}} = NP_{\mathrm{fbr}} - \ N(N-1)/2]P_{\mathrm{fbr}}^2 + \cdots \approx NP_{\mathrm{fbr}} \tag{12}$$

By the same approach the overall failure probability of the entire turbine disk can be approximated by

$$P_{\mathrm{f}\,\underset{\mathrm{total}}{\mathrm{turbine}}} \approx NP_{\mathrm{fbr}} + P_{\mathrm{f}\,\underset{\mathrm{disk}}{\mathrm{hub}}} \tag{13}$$

Note that Eqs. (12) and (13) hold only if the components and overall failure probability are small ($<10^{-2}$). For higher failure probabilities of an individual component, the quadratic or higher-order terms in Eq. (11) must be included.

Figure 17 shows the failure probability of a single blade with a 26-μm root fillet radius as a function of blade height. Applying Eq. (14) gives the overall failure probability of the microturbine. Consider a turbine disk with 20 200-μm-tall blades. The fillet radii at the hub and the blade roots are 15 and 26 μm, respectively. This is close to the values that initial fabrication experiments have yielded. The overall structural failure probability is obtained from Figs. 16 and 17 and Eq. (13) as

$$P_{\mathrm{f}\,\underset{\mathrm{total}}{\mathrm{turbine}}} = 5 \times 10^{-7} + 20 \times 2 \times 10^{-9} = 5.4 \times 10^{-7}$$

This predicted failure probability is low, although it must be recognized that structural failure is only one aspect of the device reliability. However, as the blade height is increased to 360 μm the failure probability for a single blade increases to 10^{-5}, and the overall probability of failure is raised to 10^{-4}. Although at this stage no target reliability has been set, a useful guideline is the 6σ ($\sim$3 failures in 10^6 parts) quality metric commonly used in microelectronics and elsewhere.[27]

VI. Summary

Based on the structural analysis and material strength testing, it is apparent that the design of the micro-turbine-generator rotor, although highly stressed, is feasible. However, this feasibility is very dependant on the etching process to achieve a high surface quality and hence strength. An isotropic surface finishing etch potentially provides a robust means of achieving this.

The failure probability and tip deflection increase rapidly as blade height is increased. The results presented herein permit design trades between turbomachinery performance, fabrication efforts, and structural reliability.

This paper presents the probabilistic structural design of a micro-turbogenerator. The overall approach and tests employed are equally applicable to other highly stressed MEMS applications.

Acknowledgments

The authors wish to thank the Army Research Office for financial support under ARO Grant DAAH04-95-1-0093, Technical Monitor Richard Paur. Discussions with colleagues at the Massachusetts Institute of Technology, in particular, Alan Epstein, Steve Senturia, and Martin Schmidt, are gratefully acknowledged. The authors would also like to thank Arturo Ayon for his assistance in making test specimens.

References

[1] Epstein, A. H., and Senturia, S. D., "Macro Power from Micro Machinery," *Science*, Vol. 276, No. 5316, 1997, p. 1211.

[2] Epstein, A. H., Senturia, S. D., Anathasuresh, G., Ayon, A., Breuer, K., Chen, K.-S., Ehrich, F. E., Gauba, G., Ghodssi, R., Groshenry, C., Jacobson, S., Lang, J. H., Lin, C.-C., Mehra, A., Miranda, J. M., Nagle, S., Orr, D. J., Piekos, E., Schmidt, M. A., Shirley, G., Spearing, S. M., Tan, C. S., Tzeng, Y.-S., and Waitz, I. A., "Power MEMS and Microengines," *Proceedings of IEEE Transducers '97*, Inst. of Electrical and Electronics Engineers, New York, 1997, pp. 753–756.

[3] Epstein, A. H., Senturia, S. D., Al-Midani, O., Anathasuresh, G., Ayon, A., Breuer, K., Chen, K.-S., Ehrich, F. E., Esteve, E., Frechette, L., Gauba, G., Ghodssi, R., Groshenry, C., Jacobson, S., Kerrebrock, J. L., Lang, J. H., Lin, C.-C., London, A., Lopata, J., Mehra, A., Mur Miranda, J. O., Nagle, S., Orr, D. J., Piekos, E., Schmidt, M. A., Shirley, G., Spearing, S. M., Tan, C. S., Tzeng, Y.-S., and Waitz, I. A., "Micro-Heat Engines, Gas Turbines, and Rocket Engines—the MIT Microengine Project," AIAA Paper 97-1773, June–July 1997.

[4] Spearing, S. M., and Chen, K.-S., "Micro-Gas Turbine Engine Materials and Structures," *Ceramic Engineering and Science Proceedings*, Vol. 18, No. 4, 1997, pp. 11–18.

[5] Piekos, E., Orr., D. J., Jacobson, S. A., Ehrich, F. F., and Breuer, K. S., "Design and Analysis of Microfabricated High Speed Gas Journal Bearings," AIAA Paper 97-1966, June 1997.

[6] Timoshenko, S., and Goodier, J., *Theory of Elasticity*, 3rd ed., McGraw–Hill, New York, 1970, pp. 80–83.

[7] Brantley, W. A., "Calculated Elastic Constants for Stress Problems Associated with Semiconductor Devices," *Journal of Applied Physics*, Vol. 44, 1973, pp. 534, 535.

[8] Kelly, A., and Macmaillan, N. H., *Strong Solids*, 3rd ed., Clarendon, Oxford, 1986, p. 19.

[9] Chen, P., and Leipold, M. H., "Fracture Toughness of Silicon," *American Ceramic Society Bulletin*, Vol. 59, 1980, pp. 469–472.

[10] Hu, S. M., "Critical Stress in Silicon Brittle Fracture and Effect of Ion Implantation and Other Surface Treatments," *Journal of Applied Physics*, Vol. 53, No. 5, 1982, pp. 3576–3580.

[11] Wilson, C. J., and Beck, P. A., "Fracture Testing of Bulk Silicon Micro-Cantilever Beams Subject to a Side Load," *Journal of MEMS*, Vol. 5 No. 3, 1996, pp. 142–150.

[12] van Arsdell, W., "Subcritical Crack Growth in Polysilicon MEMS," Ph.D. Dissertation, Massachusetts Inst. of Technology, Cambridge, MA, June 1997.

[13] Mura, H., Ishitsuka, N., Saito, N., Ohta, H., Hashimoto, C., and Ikeda, S., "Stress Analysis of Transistor Structures Considering the Internal Stress of Thin Films," *Japanese Society for Mechanical Engineering (A)*, Vol. 39, No. 2, 1996, pp. 166–171.

[14] Hirsch, P. B., Roberts, S. G., Samuels, J., and Warren, P. D., "The Brittle-to-Ductile Transition in Silicon," *Mechanics of Creep Brittle Materials-1*, edited by A. Cocks and A. Ponter, Elsevier Applied Science, London, 1988, pp. 1–11.

[15] Ayon, A. A., Braff, R., Lin, C., Sawin, H. H., and Schmidt, M. A., "Characterization of a Time-Multiplexed Inductively Coupled Plasma Etcher," *Journal of the Electrochemical Society*, Vol. 146, No. 1, 1999, pp. 339–349.

[16] Griffith, A. A., "The Phenomena of Rupture and Flow in Solids," *Philosophical Transactions of the Royal Society of London, Series A*, Vol. 221, 1921, pp. 163–198.

[17] Weibull, W., "A Statistical Theory of the Strength of Materials," *Vetenskaps Akad. Handl.*, No. 151, 1939, p. 45.

[18] Barnett, R. L., "Fracture of Brittle Materials Under Transient Mechanical and Thermal Loading," U.S. Air Force Flight Dynamics Lab., AFDRL-TR- 66-220, Dayton, OH, March 1967, pp. 591–619.

[19] *ABAQUS/Standard 5.5 Users Manual*, Hibbit, Karlsson, and Sorensen, Inc., Pawtucket, RI, 1996.

[20] Blevins, R. D., *Formulas for Natural Frequency and Mode Shape*, Krieger, Malabar, FL, 1984, p. 109.

[21] Spearing, S. M., "Materials Issues in MEMS," *Acta Materialia*, Vol. 48, No. 1, 2000, pp. 179–196.

[22] Hibbit, H. D., *International Journal of Numerical Method in Engineering*, Vol. 14, No. 3, 1979, pp. 937–941.

[23] Nemeth, N. N., Manderscheid, J. M., and Gyekenyesi, J. P., "Ceramics Analysis and Reliability Evaluation of Structures (CARES). Users and Programmers Manual," NASA TP-2916, Aug. 1990.

[24] Chen, K.-S., Ayon, A., and Spearing, S. M., "Controlling and Testing the Fracture Strength of Silicon at the Mesoscale," *Journal of the American Ceramic Society*, Vol. 83, No. 6, 2000, pp. 1476–1484.

[25] Chen, K.-S., "Materials Characterization and Structural Design of Ceramic Micro Turbomachinery," Ph.D. Dissertation, Massachusetts Inst. of Technology, Cambridge, MA, 1998, pp. 76–108.

[26] Pai, S. S., and Gyekenyesi, J. P., "Calculation of Weibull Strength Parameters and Batdorf Flow-Density Constants for Volume- and Surface-Flaw-Induced Fracture in Ceramics," NASA TM-100890, Oct. 1988.

[27] Harrold, D., "Designing for Six Sigma Capacity," *Control Engineering*, Vol. 46, No. 1, 1999, pp. 62, 63.

A. N. Palazotto
Associate Editor